Biologically Inspired Climbing with a Hexapedal Robot

M. J. Spenko
Mechanical and Aerospace Engineering
Illinois Institute of Technology
Chicago, Illinois 60616
e-mail: mspenko@iit.edu

G. C. Haynes
The Robotics Institute
Carnegie Mellon University
Pittsburgh, Pennsylvania 15213
e-mail: gch@cs.cmu.edu

J. A. Saunders
Boston Dynamics, Inc.
78 Fourth Avenue
Waltham, Massachusetts 02451
e-mail: aaron@bostondynamics.com

M. R. Cutkosky
Department of Mechanical Engineering
Stanford University
Stanford, California 94305
e-mail: cutkosky@stanford.edu

A. A. Rizzi
Boston Dynamics, Inc.
78 Fourth Avenue
Waltham, Massachusetts 02451
e-mail: arizzi@bostondynamics.com

Journal of Field Robotics 25(4–5), 223–242 (2008)
Published online in Wiley InterScience (www.interscience.wiley.com). • DOI: 10.1002/rob.20238

R. J. Full
Department of Integrative Biology
University of California, Berkeley
Berkeley, California 94720
e-mail: rjfull@berkeley.edu

D. E. Koditschek
Electrical and Systems Engineering
University of Pennsylvania
Philadelphia, Pennsylvania 19104
e-mail: kod@ese.upenn.edu

Received 21 November 2007; accepted 4 February 2008

This paper presents an integrated, systems-level view of several novel design and control features associated with the biologically inspired, hexapedal, RiSE (Robots in Scansorial Environments) robot. RiSE is the first legged machine capable of locomotion on both the ground and a variety of vertical building surfaces including brick, stucco, and crushed stone at speeds up to 4 cm/s, quietly and without the use of suction, magnets, or adhesives. It achieves these capabilities through a combination of bioinspired and traditional design methods. This paper describes the design process and specifically addresses body morphology, hierarchical compliance in the legs and feet, and sensing and control systems that enable robust and reliable climbing on difficult surfaces. Experimental results illustrate the effects of various behaviors on climbing performance and demonstrate the robot's ability to climb reliably for long distances.

1. INTRODUCTION

An important area of research in legged robotics concerns walking and running over challenging terrain including the ability to traverse horizontal and vertical surfaces. In comparison to locomotion over rough but substantially level ground, vertical climbing poses significantly more challenges. The robot must continually pull itself inward toward the wall while propelling itself against gravity. Even transient errors in positioning the feet or controlling their forces can be catastrophic.

Previous robots for climbing vertical surfaces have generally relied on magnets (e.g., Balaguer, Gimenez, Pastor, Padron, & Abderrahim, 2000; Xu, & Ma, 2002), suction (e.g., Lal Tummala, 2002; La Rosa, Messina, Muscato, & Sinatra, 2002; Zhu, Sun, & Tso, 2002), or specific handholds on which they can obtain a firm grip (e.g., Bretl, 2006; Kennedy et al., 2005). However, a more general and arguably more useful robot would be capable of climbing a wide variety of exterior building surfaces, including ones that are dusty and rough, where specialized attachment mechanisms such as magnets and suction fail. Such robots would be useful for surveillance, hazard removal, maintenance, and disaster relief applications.

Currently, a few machines are capable of operating on these real-world surfaces, and none has been reported that can operate on a diverse set of unstructured level and vertical terrains. One common approach to wall climbing uses a conventional skid-steered wheeled vehicle with the addition of either a device that creates a controlled vortex (Clarifying, 2006) or a negative pressure (Xiao, Morris, Chakravarthy, & Calle, 2006). These machines have been successful on brick and glass; however, they are noisy and require continuous power to maintain contact with the wall, limiting them to short missions. Spinybot (Asbeck, Kim, Cutkosky, Provancher, & Lanzetta, 2006), the first legged robot to climb flat exterior building surfaces, was successful in demonstrating the necessary attachment mechanisms but did not have the maneuverability to negotiate around

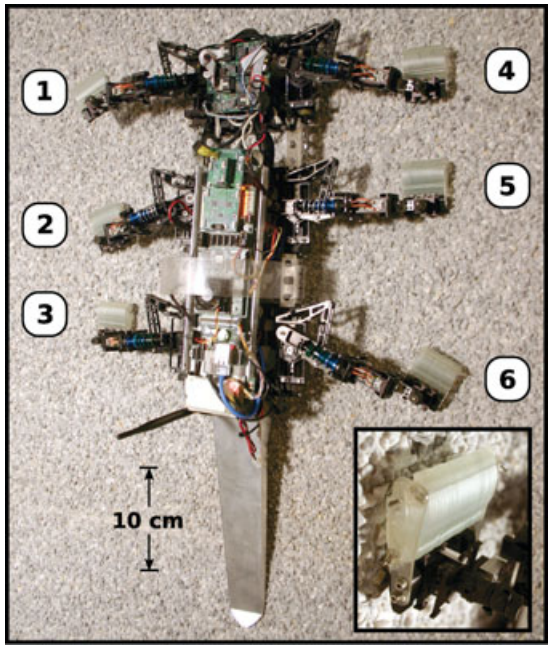

Figure 1. RiSE shown climbing a crushed stone wall using its compliant feet with embedded microspine structures. Leg numbering conventions are noted. Inset: the upper left foot (#1) attached to the surface of the wall.

or over obstacles, nor the capability to move on level ground. Spinybot pioneered the development and implementation of specialized, high mobility, passively compliant "toes" that attach to asperities on the wall. The robot presented in this paper, the hexapedal RiSE (for Robots in Scansorial Environments), first reported in Koditschek et al. (2005), is a generalist. It is capable of behavioral adaptations to a variety of appendages and climbing situations including an adaptation of Spinybot's technology (Figure 1, inset) for scaling flat exterior walls. The toes are modified to account for RiSE's considerably greater weight (3.8 versus 0.4 kg) and additional degrees of freedom (DOF), which are a necessary consequence of RiSE's greater behavioral versatility and payload capacity.

To our knowledge, RiSE is the first legged robot capable of untethered operation over diverse terrain in both the cursorial (level) and scansorial (climbing) regimes. This paper offers the first systems-level view of how the robot's novel climbing capabilities arise from an appropriate interpretation of biological insights into animal locomotion and their effective implementation in an integrated body and behavioral plan. Specific attention is paid to the interdependent design parameters pertaining to body morphology and actuation strategy (Section 2), tuned hierarchical leg and foot compliance (Section 3), and control architecture (Section 4). Further detail regarding the robot's control architecture includes methods used to generate various climbing gaits, control forces at the feet, and recover from events such as a failure of the feet to attach to the climbing surface. In Section 5 we present empirical evidence for the efficacy of this integrated design and the robot's resulting behavior, demonstrated as successful climbing on a variety of vertical building surfaces including brick, stucco, cinder block, and stone facades. We document the effects of variations in the control scheme on climbing performance. A brief assessment of the prospects for utilitarian climbing machines concludes the paper.

2. CLIMBING ROBOT DESIGN

2.1. Inspiration from Animal Climbers

Nature provides many examples of climbers that can be used as sources of inspiration. While climbing noncurved surfaces (i.e., walls, not trees or poles), animals seem to rely on a number of common principles (Autumn, Dittmore, Santos, Spenko, & Cutkosky, 2006; Goldman, Chen, Dudek, & Full, 2006):

- a flattened or sprawled posture in which the center of mass is held close to the surface to minimize the pitch-back moment;
- forces at the front limbs that pull inward, toward the wall, and forces at the rear limbs that push outward (positive normal force acting on the surface), to counteract the pitch-back moment;
- a long body and perhaps a tail to reduce the magnitude of the pull-in force required at the front limbs;
- significant lateral forces that act inward toward the central axis of the body;
- compliant legs, ankles, and toes that help to distribute the contact forces such that small perturbations in foot placement do not produce large perturbations in the forces.

In the early design stages, planar dynamic simulations were created in Working Model 2D (Design Simulation Technologies, Inc.) to evaluate the effects

of different gaits and numbers of legs (Saunders, Goldman, Full, & Buehler, 2006). The results suggested that the approach taken by insects was particularly suitable for robotic implementation. With six legs, there is a margin of safety if one foot loses its grip. Also, if the front limbs are unable to obtain a good purchase, the middle legs can provide the necessary pull-in force. A hexapod also has a wide variety of available gaits, ranging from a fast alternating tripod to a conservative pentapedal crawl, in which only one foot is removed from the surface at a time. RiSE also employs a static tail, which presses against the wall to reduce the pull-in forces required at the front limbs (approximately 1.3 N when all six feet are on the wall) (Norberg, 1986).

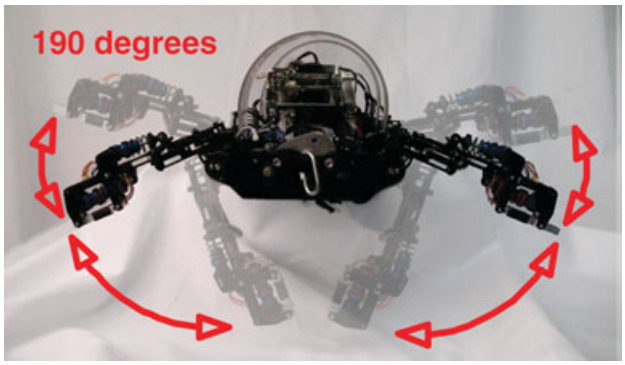

Figure 3. RiSE has a large range of motion in the "wing" DOF. This allows the robot to walk with its legs underneath its body and climb with its legs in a sprawled position.

2.2. Body and Limb Design

During the conception of the platform many of the biological observations above were known for four-legged geckos, but data pertaining to the six-legged cockroach were being collected. Consequently, it was decided to design a modular system, as seen in Figures 1 and 2, composed of three pairs of legs with spacers between the sections to adjust the overall body length and the free workspace available to each leg. Each leg is a self-contained module with two DOF under microprocessor control. This modularity incurs minimal cost in terms of weight but provides significant configuration flexibility. For example, in some experiments the middle pair of legs is removed for testing a quadrupedal configuration.

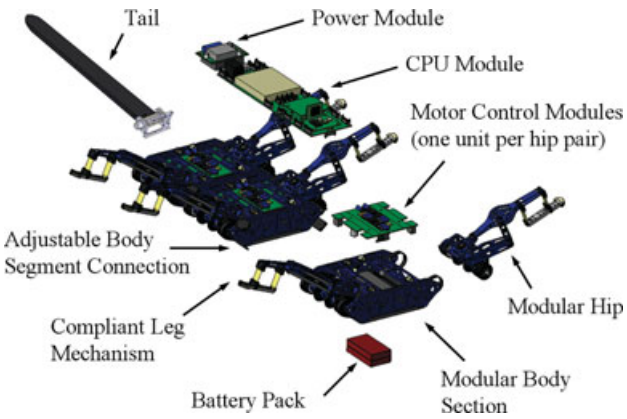

Figure 2. RiSE's modular design allows for easy reconfiguration of the different leg segments. Each module contains four motors, a four-axis motor amplifier, and one battery pack.

Some animals, e.g., squirrels, that frequently switch between running and climbing often adopt a "crouched" configuration with the legs below the body for running, and a "sprawled" configuration for climbing. Although this differentiation in body posture is likely advantageous to larger animals (>1 kg), it is a necessity for RiSE given the incapability of its dc motors to provide enough torque to both support the body weight and move forward if RiSE were to use a sprawled posture on level ground. In RiSE this adaptability is achieved using the abduction/adduction or "wing" DOF as shown in Figure 3. To improve climbing performance, heavy components such as batteries and motors (which make up 55% of the robot's mass) are placed as close to the underside of the robot as possible so that the center of mass is just a few centimeters from the surface of the wall.

For a given robot mass, trade-offs need to be made between the number and DOF of the legs and maneuverability of the robot. Weight constraints for the robot are a function of the climbing substrate's strength and the ability to distribute the robot's mass onto that substrate (as described in Section 3). To determine the available number of actuated DOF per leg, we must first estimate the power required to climb against gravity, given by

$$P_l = \frac{mgv}{\eta N_l}, \tag{1}$$

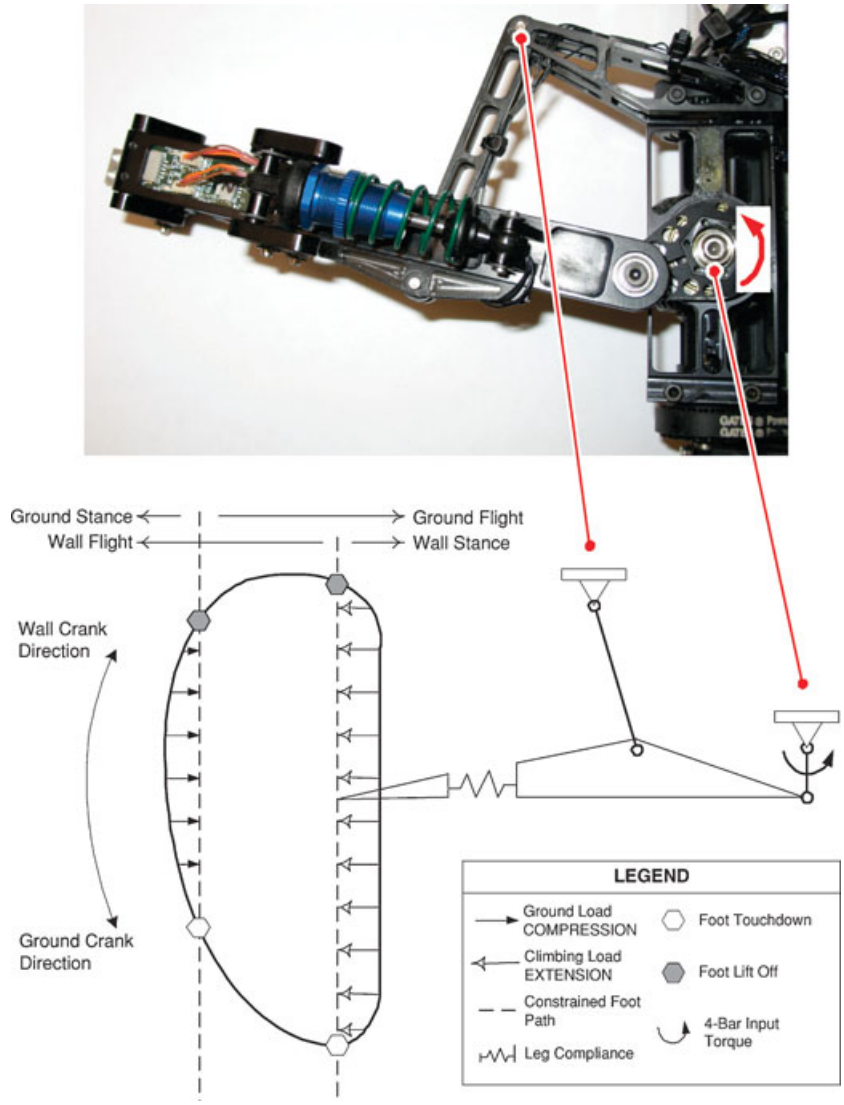

Figure 4. Picture of a single RiSE leg with the corresponding schematic detailing the linkages and foot path of the "crank" DOF.

where η is the drivetrain efficiency, assumed to be 50% based on previous experience with similarly sized robots. The target mass m of the robot was 2 kg, and the target velocity v was 0.25 m/s. Assuming a worst-case situation, there could be only two feet in contact with the wall: $N_l = 2$. Thus, at least 5 W of mechanical power per leg is required. However, there are additional losses associated with foot placement and the processes of climbing. For example, Autumn, Hsieh, Dudek, Chen, Chitaphan, and Full (2006) measured the effective acceleration against gravity for vertically climbing geckos and observed that they generate a total mechanical energy that exceeds the change in potential energy by up to 15%. Taking this into consideration requires on the order of 6 W of mechanical power per leg; however, motors with this power rating did not provide enough stall torque to apply adequate lateral forces to "grip" the surface and perhaps adjust the posture of the body. Because more than one DOF per leg is required to produce

the desired ground reaction forces, each leg uses two Maxon RE16 4.5-W motors with enough combined power to grip the surface while climbing vertically. Maxon's rated power is used as a selection guideline, whereas the actual mechanical power available is a function of several parameters including gear train efficiency, heat dissipation, and duty cycle.

With an initial target weight of 2 kg and the choice of a hexapedal configuration, the weight budget permitted only two actuators per leg. As a result, the key to locomotion in both vertical and horizontal terrain with the same underactuated leg mechanism was to exploit a foot path generated by a four-bar crank-rocker mechanism in combination with passive leg compliance. Figure 4 shows a planar view of one leg, along with the corresponding trajectory for the linkage.

An interesting feature of the linkage is that the crank rotates in opposite directions for level ground locomotion and climbing. This design feature is a result of the discovery that running animals always push out with their legs, such that the ground reaction force vector points back along the leg. Legged animals on the level bounce side to side (Chen, Peattie, Autumn, & Full, 2006). When legged animals climb, these forces reverse so that legs always pull in (Autumn, Dittmore, et al., 2006).

While locomoting on the ground, the foot follows an anticlockwise path such that the outer, curved, portion of the trajectory represents the ground contact phase. In conjunction with the passive compliance along the lower limb, this leads to a moderately fast (0.25 m/s) alternating tripod gait as seen in many animals. For climbing, the crank rotation is reversed and the inner, nearly straight portion of the path is utilized to pull the robot upward along the wall. The straight path helps to prevent excessive variations in the contact forces between the foot and the wall. Note, however, that while the tip of the leg traces a nearly straight line, it also rotates. Therefore, rotational compliance is needed at the ankles so that the feet can caster, as discussed in Section 3.2.

Leg compliance is achieved using readily available shock absorbers for small radio-controlled vehicles. Figure 5 shows a front view of one leg. The shock absorbers are mounted in opposition and connected to a passive parallel linkage that extends or retracts to increase or decrease the radial length of the leg. Because there is no motor associated with this radial DOF, it is important to be able to adjust the leg compliance to match the weight of the robot. If the compliance is too low, excessive lateral forces will result, causing the feet to lose their grip; if it is too high, the robot will sag outward, pitching back from the wall. This tuning of the leg compliance is independent of the climbing substrate.

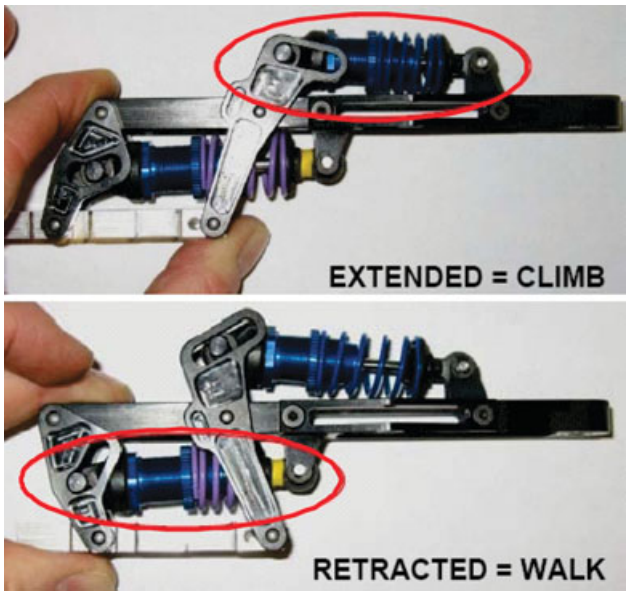

Figure 5. Extension and compression of the leg is composed of two independent shock absorbers. The upper shock controls the spring and damping parameters for leg extension and thus is most important in climbing when RiSE must generate ground reaction forces that help stabilize the robot. The lower shock acts in compression and is tuned for walking.

Each of the six leg mechanisms is powered by two geared servo motors. A differential hip mechanism enables the actuators to drive the two-DOF leg mechanism while minimizing leg mass (less than 2.5% of the body mass); see Figure 4. This configuration keeps distal leg mass low, which reduces foot impact forces and inertial effects.

The differential allows the two actuators to control the two-leg DOFs either independently or simultaneously. When both motors are driven in the same direction at equal speed, the wing, or abduction/adduction, DOF is actuated (Figure 3). When the motors drive in opposite directions at the same speed, the crank of the four-bar mechanism is actuated, causing the foot to follow the path depicted in Figure 4. Any other combination of directions and speeds actuates both DOFs simultaneously.

Additionally, as a result of this coupling, both motors can share the load of either DOF. This helps reduce the total required mass of the actuators as each motor does not need to be sized for the worst-case loads of each DOF. This is particularly useful for flat surfaces where the two DOF are generally used sequentially. However, on highly curved surfaces such as poles or small trees, the two DOF may require substantial power at the same time, reducing the advantage of the differential.

2.3. Sensing and Computation

Onboard electronics control the leg motion, manage communications, and service a variety of sensors. The platform is computationally autonomous; communication to the operator control unit (OCU) is achieved through a wireless 802.11 link, allowing the robot to be guided remotely. Owing to the small size of the RiSE platform, a custom electronics suite was designed to integrate a small-form-factor personal computer, memory, and a solid-state inertial measurement unit. Similar constraints led to the development of a compact high-frequency amplifier to drive the low inductance coreless dc gearmotors.

Distributed signal processing enables better integration of sensors with the mechanical structures and reduces wiring complexity. The processor for each leg is a Cygnal C8051F021 microprocessor, with C8051F330 processors for monitoring the force sensors at each leg. The other sensors include joint position sensors for each leg, motor current sensors, and Hall effect sensors for joint limits and the inertial measurement unit. On-platform communication and control is achieved through a custom, serial-based, distributed communications protocol referred to as RiSEBus built atop I^2C and ISA bus components. It is used to connect sensors and motor control boards to the CPU module. The main controller runs under a real-time Unix operating system and has an update period of 4 ms.

As legged robots progress from running over level ground to climbing increasingly steep slopes, the control of forces at the feet becomes increasingly important. In the case of RiSE, force control ensures that no foot is loaded too heavily, which could cause it to lose its grip or incur irreparable damage. Force sensors are also useful for indicating when a foot has made or lost contact with the climbing surface. The incorporation of force sensing in the control algorithms is discussed in Section 4. Force sensing for the fore–aft and adduction/abduction directions is accomplished with strain gauge load cells built into the lower legs (Figure 6), which measure forces normal and tangential to the feet. The measured forces are accurate to within 0.25 N. A less accurate system, consisting of a Hall effect sensor measuring the passive compliant deflection along the leg axis (Figure 5), provides a third axis of force measurement accurate to approximately 0.5 N, due to hysteresis in the shock absorbers. Although it is conceivable that environmental contamination in the form of dirt and grime could affect the hysteresis and accuracy of the force sensors, we have found no such effect in practice. Analog signals from these sensors are conditioned and read by each leg's associated microprocessor, which communicates the calibrated force measurements to the central processor.

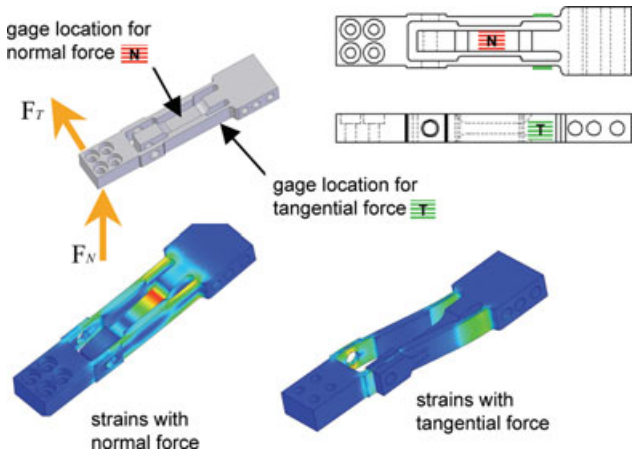

Figure 6. Strain gauges are incorporated into the lower legs for force sensing in the actuated DOF. F_N corresponds to the adduction/abduction direction; F_T corresponds to the fore–aft direction.

2.4. Platform Capabilities

The platform currently weighs just over 3.8 kg and has a payload capacity of 1.5 kg. Three onboard lithium polymer batteries power the control and motor circuitry and provide run times in excess of 45 min. Control and data logging are achieved through standard 802.11b with a line-of-sight distance (using standard consumer network equipment) of up to 30 m.

The robot is capable of traversing a variety of vertical and horizontal terrains (Figure 7). The full array

Figure 7. The RiSE platform is capable of scaling a wide variety of real-world surface types and variations as well as maintaining capable level-ground locomotion. Clockwise from the upper left, RiSE climbing a tree, climbing a brick wall, and walking through tall grass.

of surfaces makes use of three styles of feet. For walking on horizontal surfaces, spherical rubber feet are attached and speeds up to 0.25 m/s are obtained. In the next section, we describe the feet and attachment mechanisms used for climbing soft and hard vertical surfaces.

3. SPINY FEET FOR CLIMBING

The mechanisms that allow RiSE to climb are inspired by scansorial animals, which have developed a range of approaches for maintaining contact with a wide variety of surfaces (Spagna, Goldman, Lin, & Koditschek, 2007). These strategies can be divided into two categories: interlocking and bonding mechanisms (Cartmill, 1985). Interlocking solutions such as claws or spines generate a combination of pull-in and propulsive forces against gravity either by penetrating surfaces or by latching onto small asperities (bumps or pits) on the surface. Most larger climbing animals such as cats and bears use penetrating claws. In contrast, bonding mechanisms generate adhesion via suction, chemicals, capillary forces, or van der Waals forces. In general, smaller animals such as lizards, frogs, and insects use bonding; however, many of these animals use a combination of the two methods.

RiSE uses both interlocking mechanisms (spines and claws) and bonding (smooth adhesive patches) and is thus capable of climbing both rough and smooth surfaces (Spenko et al., 2006). However, RiSE's current performance on smooth surfaces is limited to inclines of 65 deg, and thus this paper focuses on climbing rough 90-deg surfaces using interlocking structures.

The two interlocking mechanisms that RiSE uses are distinguished by the method with which they engage the surface. Claws are hard nail-like structures with no compliance that create asperities by penetrating the climbing substrate. They are useful for climbing trees and other soft surfaces. The load/penetration characteristics of these single-point claws are discussed in Provancher, Clark, Geisler, and Cutkosky (2005) and depend significantly on the approach angle and claw tip radius. Spines are characterized by a tuned compliance between a metal hook that engages with asperities on the climbing surface and the body of the robot. Spines are used on hard surfaces such as concrete, where penetration is not practical. The spines work by sliding and catching on asperities such that the coefficient of friction between the spine tip and surface makes it possible to apply a combination of vertical and pull-in forces. The spines used on RiSE are adapted from an earlier design (Asbeck et al., 2006) and draw their inspiration chiefly from the spines found on insect legs (Figure 8) and whose utility has been previously found to be effective for level-ground robotic locomotion (Spagna et al., 2007). Even animals such as the gecko, with its vaunted adhesive system, often use distal toe claws when climbing rough rock (Zani, 2000).

For the spines to work, they must have a tip dimension comparable to that of the asperities that they catch, i.e., with a tip radius on the order of tens of micrometers (Asbeck et al., 2006). Because the spines are small, each spine is capable of supporting a relatively small load (a few newtons at most), and many spines are needed to support the 3.8-kg RiSE platform. As described in the following sections, a hierarchical system of compliances is used to ensure that the spines can be presented to the surface and then loaded properly and that the weight of the robot is distributed evenly among them.

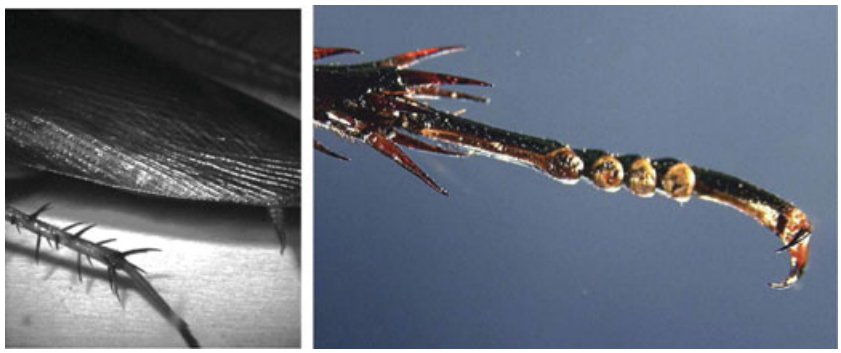

Figure 8. (Left) Insects' legs are equipped with numerous small spines that catch on asperities, helping them to climb. The spines are often directional, stiff when the leg pushes but flexible when it retracts. (Right) A tarsal claw resides at the end of a cockroach's leg.

3.1. Compliant Multimaterial Appendages

There have been several iterations of feet and toes for RiSE. Currently RiSE uses the 10th- and 11th-generation toes (Figure 9). Each foot is composed of 25–50 flat toes arranged in a row. The total number of toes is related to the thickness of the hook or spine used and loosely correlated to density of asperities on the climbing surface. The relationship between asperity density, the strength of the spine/asperity contact, and the mass of the robot is detailed in Asbeck et al. (2006). The 10th-generation toes (Figure 9, left) have spines that are made from fishhooks (Tiemco TMC 100BL) with a tip radius of approximately 25 μm. These toes climb well on surfaces with larger asperities such as brick and stone facades. The 11th-generation toes (Figure 9, right) have smaller spines (Finescience 26002-10), with a tip radius of approximately 15 μm, and perform better on surfaces with small asperities such as concrete cinder blocks.

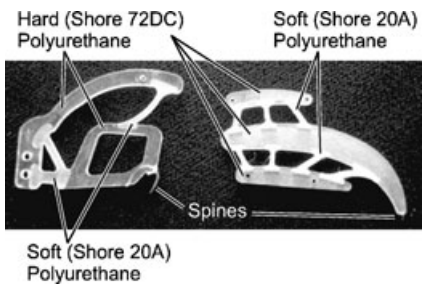

Figure 9. Tenth (left) and eleventh (right) generation of toes used on RiSE.

Each toe is a multibar elastic linkage composed of two grades of polyurethane (Shore 20A and Shore 72DC) and is manufactured using Shape Deposition Manufacturing (SDM) (Weiss et al., 1997). The multiple grades of polyurethane allow the toe both to stretch tangentially along the wall and to compress normally, away from the wall. When contacting the wall, the compliance in the normal direction ensures that the normal force is small, so that it does not tend to push the robot off the wall. Subsequently, the foot is dragged lightly along the wall surface, engaging the spines. Compliance in the fore–aft direction ensures load sharing among the toes.

3.2. Ankles

The next level of compliance above the toes is at the ankles (Figure 10). The ankles are designed to exhibit anisotropic stiffness centered around a universal

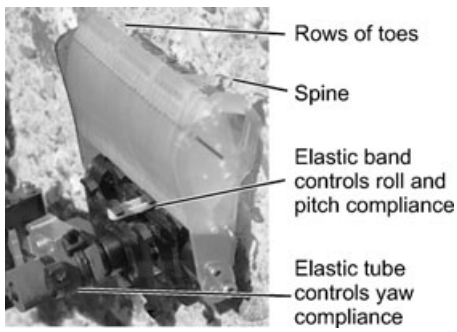

Figure 10. Ankle and foot design of RiSE.

joint. The pitch DOF is relatively stiff compared to the roll and yaw DOF. This allows the tips of the toes to maintain contact with the climbing surface. If the pitch DOF were too compliant, the toes would tend to rotate around the point of contact and disengage with the surface. The roll DOF is kept as compliant as possible to allow the entire width of the foot to engage with the climbing surface. Yaw is also relatively compliant so that as the leg goes through the stance phase, it remains aligned with the surface. The yaw angle of the foot relative to the climbing surface is determined when the foot initially contacts the surface. This angle can easily be adjusted as a function of the gait. The various levels of stiffness are achieved using an elastomeric tube and bands situated around the universal joint.

4. BEHAVIORAL CONTROL

To climb vertically, the RiSE robot takes advantage of its unique body design and foot attachment mechanisms to generate ground reaction forces that approximate those observed in biological climbers (Autumn, Hsieh, et al., 2006; Goldman et al., 2006). Given the inherent uncertainty and complexity of foot–surface interactions, we use abstractions of behavior in RiSE's control approach. RiSE uses an open-loop gait, a strategy commonly used with dynamic quadrupedal and hexapedal robots (Altendorfer et al., 2001; Cham, Bailey, Clark, Full, & Cutkosky, 2002; Poulakakis, Smith, & Buehler, 2005), to achieve these ground reaction forces.

An open-loop gait by itself is not robust to locomotive errors. Thus, feedback behaviors are added to the gait strategy in the form of force regulation. Although feedback and reactive control laws by themselves can be applied to generate full locomotive behaviors (Brooks, 1989; Cruse, 1990; Dürr, Krause, Schmitz, & Cruse, 2003; Espenschied, Quinn, Chiel, & Beer, 1993), we have found that such control systems become complex and involve an unintuitive design process. For RiSE, the feedforward gait is designed to generate the desired ground reaction forces, while the feedback controllers attempt to guarantee that these forces occur.

4.1. The Gait

Two constraints drive the design of RiSE's open-loop gait. First, the feet must apply sufficient force in the fore–aft direction to counteract gravity and propel the body upward. Second, to keep the robot attached to the wall as firmly as possible, the maximum number of feet (consistent with the specified leg circulation pattern) must maintain contact with the substrate.

4.1.1. Gaits and Gait Parameters

An open-loop gait repeats the same leg motions, and thus the gait function can be represented as a periodic mapping from the phase of an oscillator, $\phi \in S^1$, to the desired configuration of the robot's joints (Haynes & Rizzi, 2006a; 2006b). If the robot's configuration space is denoted as $\mathbb{Q}$, then a gait g is a periodic function that can be represented as an embedding of the circle:

$$g : S^1 \to \mathbb{Q}. \tag{2}$$

For ease of gait design and debugging, it is attractive to introduce a "parallel" and a "sequential" decomposition of the gait function g. The parallel decomposition splits a gait into the motions for each leg, rather than the whole body, creating six constituent functions, each an embedding of the circle into the jointspace of leg, $g_i : S^1 \to \mathbb{Q}_i$ so that

$$g(\phi) = \begin{bmatrix} g_1(\phi) \\ \vdots \\ g_6(\phi) \end{bmatrix}. \tag{3}$$

The sequential decomposition further promotes a distinction between the temporal and spatial aspects of a leg's trajectory during a stride. We will denote this as $g_i = g_{i,s} \circ g_{i,t}$, where $g_{i,t}$ is a diffeomorphism of the circle, $g_{i,t} : S^1 \approx S^1$, and $g_{i,s}$ is an embedding of the circle in the leg's jointspace.

$$g_i(\phi) = g_{i,s} \circ g_{i,t}(\phi). \tag{4}$$

The temporal component $g_{i,t}$, the clock mapping, dictates the relative speeds of legs during flight, attachment, stance, and detachment, whereas the relationships between the different clock maps, $\{g_{1,t}, \ldots, g_{6,t}\}$, determine the relative phasing of these events among the various legs. The spatial portion of a gait, $g_{i,s}$, a leg trajectory, maps the various phase intervals into the appropriate segments along the closed curve representing the desired geometric foot path.

A block diagram summarizing these parallel and sequential compositions is presented in Figure 11.

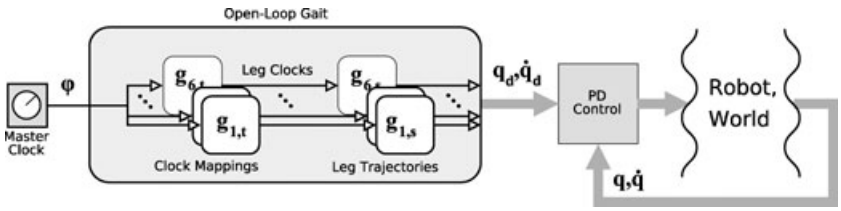

Figure 11. Open-loop gaits and their decomposition into temporal and spatial portions.

4.1.2. Spatial Gait Tuning

The process of tuning the spatial parameters of a gait involves designing a set of cyclic leg trajectories that properly engages the robot's feet with a given surface. For this reason, each tuned set of parameters is specific to a given task. Tuning involves shaping one such function—in our work, we use piecewise linear functions on joint angles, with cubic smoothing—and testing on a given surface until sufficient success is achieved.

Figure 12 illustrates the workspace of one of RiSE's legs. Each leg in the climbing gait uses a spatial trajectory built upon the same four-vertex cell partition depicted in Figure 13, tuned to properly attach the feet to the surface, load the compliance in the toes, and generate upward propulsive forces until recirculation.

The gait is designed to recruit the crank joint to engage microspines and produce traction forces while climbing. Traction force is aligned in the fore–aft direction and is along the path a foot takes when the four-bar mechanism is actuated via the crank DOF (see Figure 4). After making contact with the surface, the crank joint turns faster to engage the

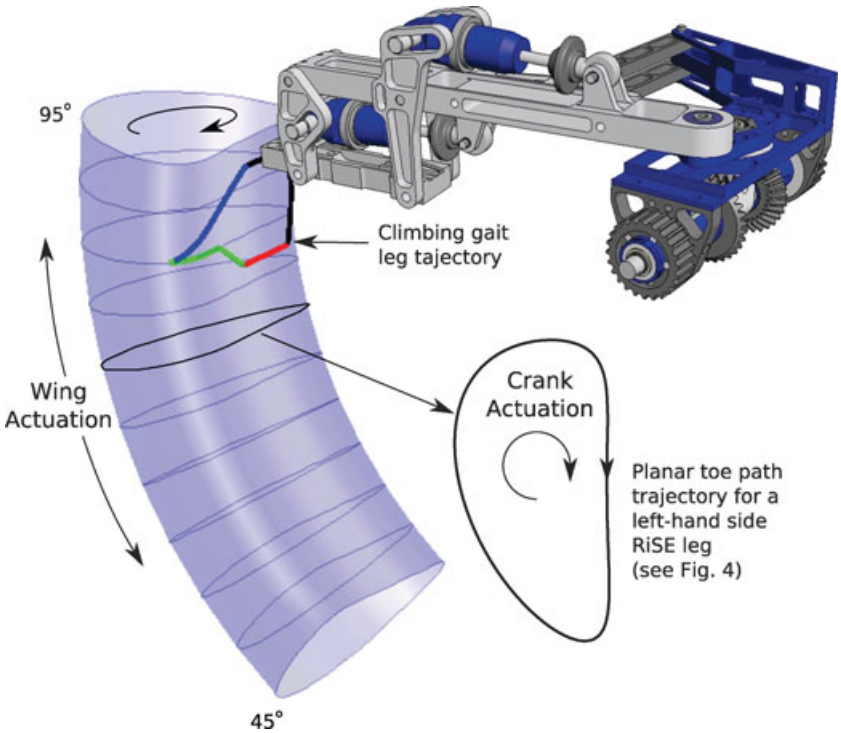

Figure 12. The two leg joints combine to parameterize a two-dimensional manifold of allowable foot positions. The leg joint trajectory corresponds to a loop on this manifold. A physical robot leg (first shown in Figure 4) is shown for comparison.

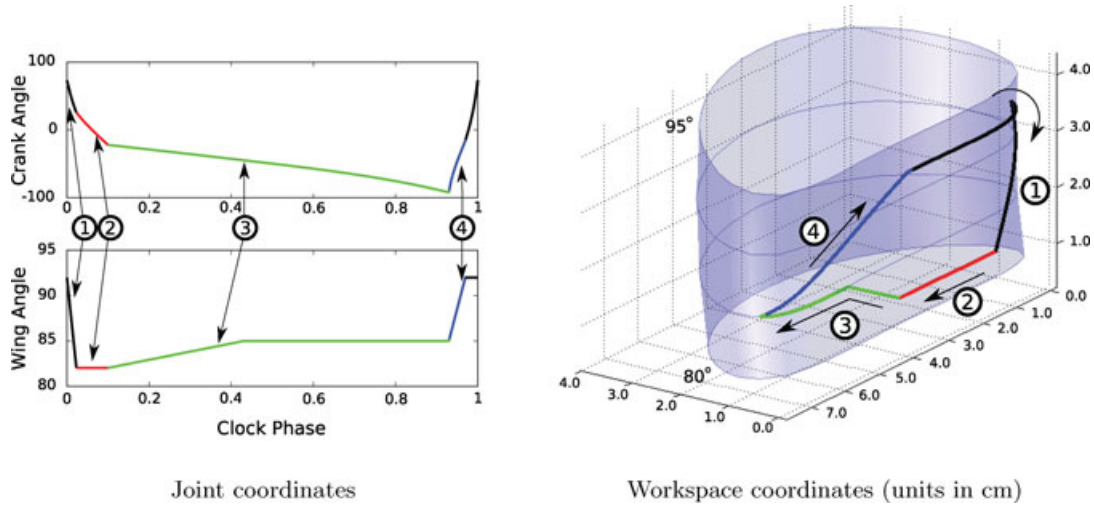

Figure 13. A single foot's trajectory, shown in joint and body frame coordinates. In body frame coordinates, a bounding box of the trajectory is shown, with units in centimeters. The sequence of events is as follows: (1) the robot lowers the wing joint to present a foot to the surface; (2) the attachment stroke drags a foot along the surface to engage it; (3) the foot enters stance and generates pull-in and fore–aft force; and (4) the crank direction reverses while the foot is lifted away from the surface, both unloading compliance and beginning recirculation.

spines, and then slower during stance to propel the robot up the wall. At the end of the stroke, the crank reverses to unload the leg compliance and disengage the spines before the leg recirculates. This sequence of steps is seen in the plots of Figure 13.

The normal force of a foot plays a crucial role in climbing and is largely tuned by adjusting the gait parameters determining the wing joint trajectory. The foot first produces a positive force when it strikes the surface. Pull-in force (negative normal force) is necessary to keep the robot's body close to the wall, and the wing joint is used to perform this task, increasing after the feet are attached.

RiSE's other scansorial behaviors, discussed in Section 2.4, make use of the lateral compliance found in the legs. The climbing behavior described here, however, uses only the normal and fore–aft compliance found in the toes. Additional lateral compliance would add more robustness to foot attachment but is currently limited by the relative strength of the toes and by the yawing rotation required by a foot during the stance phase.

4.1.3. Temporal Gait Tuning

When designing the timing of an open-loop gait, there are two important parameters to consider: the percentage of a stride each leg should be in contact with the surface (the duty factor) and the relative timing among legs (the stance phase offsets). Various choices for these parameters result in different gaits (Haynes & Rizzi, 2006b).

Owing to the robot's large mass and the limited strength of the microspines, a gait that keeps five of six legs attached at all times is used on especially challenging surfaces. For a hexapod, this corresponds to a duty factor of $^5/_6$ and phase offsets that are separated by $^1/_6$. The wave gait is one example and recirculates only one leg at any given time, shown in Figure 14.

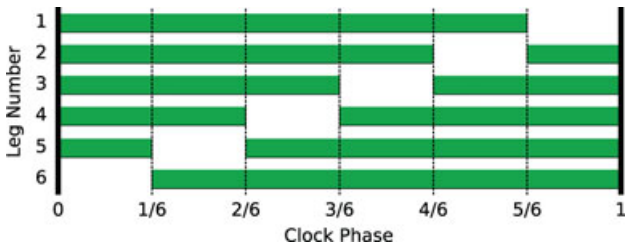

Figure 14. The timing of stance and flight for legs in a wave gait, used for open-loop static climbing with the RiSE robot. This gait keeps five legs in stance, represented by the shaded regions, at all times. The leg recirculation order is repeated for each stride of the gait.

4.1.4. Integration and Tuning

The integration of these two components—the temporal portion, which dictates when each foot begins stance and later recirculates, and the foot path trajectories encoded within the spatial portion—results in a whole body motion that can be used to climb surfaces without sensor feedback. A proportion-derivative control loop, shown in Figure 11, is used to follow desired motions, and gait parameters are tuned manually to achieve effective climbing.

4.2. Force Regulation

Having embraced a controller design organized around the feedforward gait generator presented in the preceding section, we must now incorporate some means of correcting its command outputs in response to tracking errors or more severe problems. In conventional control settings it is a well-justified tradition to introduce feedback laws based on some model of the "plant" being regulated. However, in our application, the environment (highly compliant linkages engaging completely unknown and unmodeled substrates) seems too complex and uncertain to justify that step. Thus, we have used intuition and empirical judgment to design a feedback suite that accomplishes the basic task.

We now detail our empirical approach to meeting this challenge, which uses simple feedback rules to correct for errors in both traction and normal force generation during stance. These feedback terms apply local modifications to parameters of the feedforward gait. Echoing the decomposition of the gait function, different projections of the sensory measurements are assigned influence over distinct sets of parameters that determine the functional properties of the various feedforward constituents. For the sake of completeness we briefly describe the sensory measurements used to modify the output of the temporal component but defer to Haynes & Rizzi (2006a) for a more detailed technical discussion of this mechanism because it entails the design of coupled oscillators that goes well beyond the scope of this paper. In contrast, the sensory data that largely influence the geometric components of the gait function are more straightforward to discuss, and we present them here for the first time.

4.2.1. Traction Force Controller

Traction force feedback applies load sharing across various feet while climbing. The importance of preventing any individual foot from carrying too much or too little force arises from both the fragility of the substrate and the need to protect the microspine toes. On many interesting surfaces, the roughness associated with asperities that offer useful toeholds may also incur a brittleness that requires load sharing across as many toes as possible. In any case, if an individual toe carries too much force, its compliant elements may elongate past their ultimate tensile strength, resulting in permanent damage, or be forced to disengage via a hard-stop mechanism. In contrast, a foot that is loaded too little can slip due to insufficient engagement with the surface.

The controller adjusts the gait as a function of the difference between the foot traction force and the average foot traction across all feet at a given time. The average foot force is given as

$$a_t = \frac{\sum_i f_{t,i}}{n}, \tag{5}$$

where $f_{t,i}$ is the traction force of leg i and n is the number of legs in contact, $n \leq 6$. Each foot in stance is then compared against this average. Because the spatial trajectory of a leg moves in the traction direction, speeding up an individual leg in relation to the other legs will further load the microspines on its toes. Conversely, retarding a leg will reduce its load. A proportional controller that varies leg velocities based on the relationship between the traction force and average traction force is given as

$$b_{t,i} = k_p(a_t - f_{t,i}). \tag{6}$$

Leg speed is modified by applying $b_{t,i}$ to a leg's stance phase offset, a component of the internal state of the coupled oscillator system, originally conceived in Klavins and Koditschek (2002) and applied to this robot as discussed in Haynes and Rizzi (2006a). Data from a sample run of this controller for a single leg, using a discrete version of Eq. (6), is shown in Figure 15. The leg speeds up or slows down in response to the measured forces that lie outside of a deadband region. The deadband region lies between 85% and 120% of the desired force, in which no controller action is taken. Outside of this deadband, if measured force is too low, the leg velocity increases by 70%—via a modification to the phase offset—or

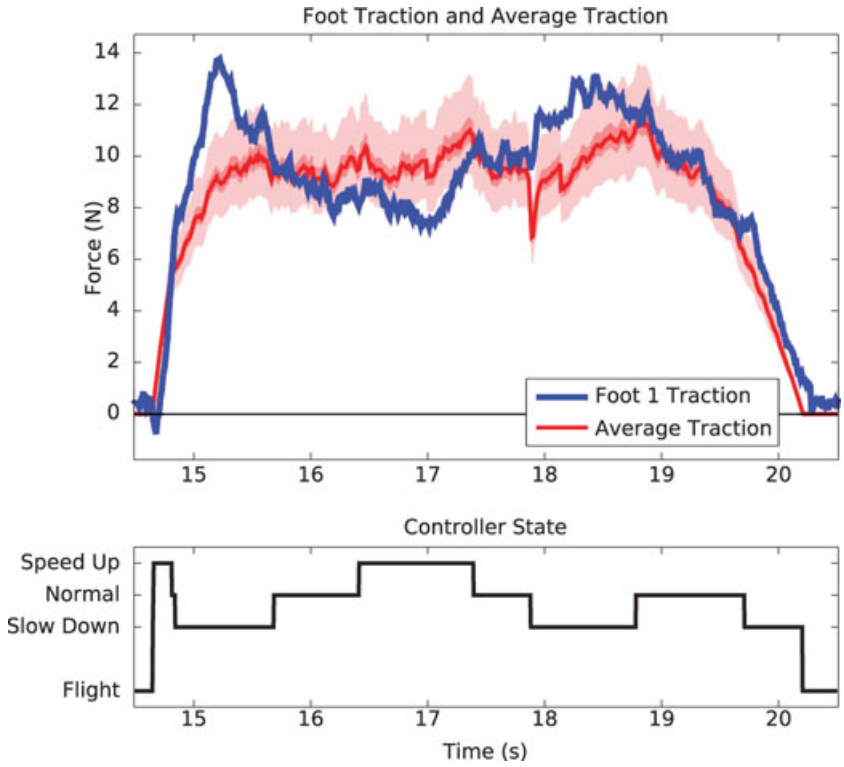

Figure 15. Result of applying traction force controller to a single leg. The top plot shows the actual force measured at a foot, as well as the desired force over the stride. The shaded region notes the deadband region. The bottom plot shows the controller action.

alternatively slows by 41% when force is too high. These values were tuned empirically.

4.2.2. Normal Force Controller

In contrast, a normal force controller that adjusts the wing limits of the geometric component of the gait function, $g_{i,t}$, is used to guarantee that feet make contact with the wall before attempting to load the traction force. Sometimes problems can occur when a foot is unexpectedly far from the surface, often due to the robot pitching back or due to surface irregularities. If the foot fails to make contact, the critical chain of steps that are designed into the open-loop gait—generate normal force, load traction force, and generate adhesion—is broken. To address this challenge, the wing angle is lowered until the foot "feels" the surface (1 N of force is measured in the normal direction). This is done by adding an extra wing angle offset to the position commanded by the open-loop gait. After 1 N of normal force is registered, the leg returns back to the nominal wing angle, causing the robot to be pulled into the surface. This step helps to correct for pitch errors and generate adhesion force.

4.3. Additional Control Techniques

The two feedback control techniques described thus far regulate contact forces for each foot, resulting in the robot having a better grasp of the climbing surface. Through experimentation, we found the addition of several other components to be helpful, and often critical, to the robustness of the climbing system. These include a pawing controller that attempts to regrasp the surface when feet accidentally slip, a method of turning that uses the traction control described above, and gait regulation to keep the robot using statically stable gaits.

4.3.1. Pawing Controller

An individual foot can occasionally fail to grasp the climbing surface after initial contact, upon which the robot executes a "pawing" strategy (Dürr, 2001).

Attachment failures often occur when a foot slips while trying to attach and can be associated with bare spots where attachment is difficult. Pawing attempts to reattach the foot both quickly and in a slightly different location on the climbing surface by quickly recirculating the foot. Unlike the two strategies above that make differential adjustments to the gait, pawing discretely changes gait parameters.

Pawing can occur throughout the stance section of the gait. Thus, when the leg is recirculating, the leg clock needs to be reset. This new offset to the leg clock is calculated by comparing the current phase to the phase at which detachment occurs. Position offsets are added to joint angles to maintain continuity of commanded positions and are computed as follows: If $g_i(\phi_d)$ are the normal joint positions of a leg at the beginning of detachment and $g_i(\phi_p)$ are the joint positions at the beginning of a pawing behavior, then $g_i(\phi_p) - g_i(\phi_d)$ are position offsets that allow the robot to execute the detachment stroke starting at the pawing position. When detachment occurs, the position offset is reduced to zero while the leg recirculates. When the leg attaches, the leg returns to the nominal trajectory. An example of a pawing motion is shown in Figure 16.

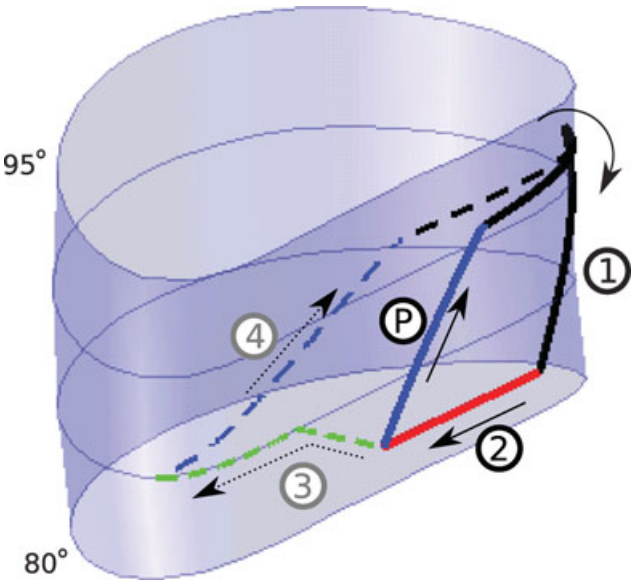

Figure 16. A leg may exhibit a pawing behavior after recirculation and attempted attachment, steps (1) and (2). Unlike the trajectory shown in Figure 13, a pawing leg will, upon sensing failed attachment, skip steps (3) and (4) by lifting up earlier, (P), in order to recirculate and retry attachment.

4.3.2. Turning Control

RiSE occasionally yaws to one side due to small slips per side during climbing. If uncorrected, the robot will continue to turn toward that side. To alleviate this problem, as well as have higher level control of the climbing, a simple strategy for turning was implemented.

A previous method for turning is discussed in Haynes and Rizzi (2006b), in which the robot alternated between its normal gait and specific "turning" gaits. This approach was difficult to tailor to the adaptive gait systems described here because it assumed that the robot was using fixed gaits. A better strategy is to make use of the traction force controller (Section 4.2.1). The traction force controller equalizes the foot force by comparing the individual foot forces to the average foot force. By modifying that average value for the set of right or left legs in proportion to the heading error, the robot will generate higher forces on one side of the robot compared to the other side. This naturally turns the robot because the legs on one side are moving faster than those on the other side and the imbalance of forces introduces a small torque.

4.3.3. Gait Regulation

Feet in contact with the climbing surface have various constraints due to their interactions with the surface. Legs in flight, however, have no constraints. This freedom allows the use of one additional control technique, gait regulation, which actively modifies the timings of the legs in flight.

Whereas the open-loop strategy uses a wave gait to climb, we have introduced control systems that modify leg speeds (via traction force control) or discretely modify a leg's timing (when pawing). These modifications could cause disastrous problems if certain legs accidentally recirculate together (i.e., all the legs on one side of the robot lift off at the same time). By speeding and slowing legs in flight, we can attempt to guarantee that only one leg recirculates at a time. This type of control is presented as a coupled oscillator system and described at length in Haynes and Rizzi (2006a). When using gait regulation, the robot tends to approximate pentapedal gaits, which keep five legs in stance at all times. While legs can swap order due to traction control or pawing, the gait regulation system keeps them separated in phase.

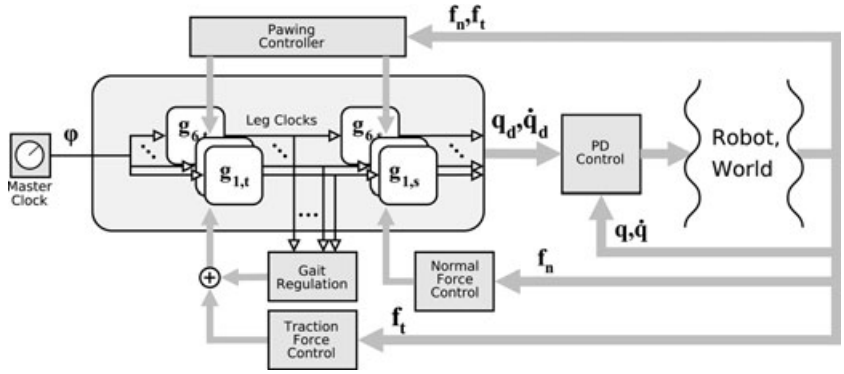

Figure 17. The use of feedback controllers in addition to the open-loop control technique, as presented in Figure 11. Force regulation (both traction and normal) as well as gait regulation supply continuous modifications of the gait output, while the pawing behavior creates impulses to suddenly change the active gait strategy.

4.4. Summary

RiSE is issued speed and turning commands from a human operator, which are fed into an integrated control strategy consisting of feedback controllers overlaid onto an open-loop gait. Traction force control and gait regulation affect leg speeds in stance and flight, respectively, while normal force control makes adjustments to joint angles. Pawing modifies gait parameters to execute a recovery motion on the onset of poor foot attachment. The integration of all of these systems is shown in Figure 17 and results in robust and reliable climbing.

5. RESULTS

RiSE is able to both walk on the ground and climb a wide variety of surfaces. To date RiSE has successfully climbed trees as varied as oak, eucalyptus, pine, and redwood. RiSE has climbed a number of man-made surfaces including brick, stucco, cinder block, and crushed rock. Rather than present results for each surface that RiSE has successfully climbed, this section details how each of the behaviors described in Section 4 affects RiSE's climbing performance, with a particular focus on exterior building surfaces using the "spiny feet" described in Section 3. The results show that when all of the behaviors are utilized, RiSE is able to climb long distances (on the order of tens of meters) without failure.

5.1. Experimental Procedure

The performance of the robot and effectiveness of the feedback behaviors described in Section 4 were experimentally validated. Both the effect of individual behaviors and combinations of behaviors were evaluated. The various controller arrangements tested were as follows:

Open-Loop Gait (OL): the robot moves its legs using cyclic feedforward motions, with no task-level feedback; Section 4.1.
Traction Force (T): the open-loop gait is augmented with traction force control, which causes the feet to vary speed while in stance; Section 4.2.1.
Normal Force (N): the open-loop gait is additionally searching for the climbing surface, measured via normal force; Section 4.2.2.
Pawing (P): the open-loop gait is run; however, if a foot fails to contact the surface, pawing causes it to retry; Section 4.3.1.
Traction Plus Gait Regulation (T+GR): similar to T, but with the addition of gait regulation to keep the legs out of phase; Sections 4.2.1 and 4.3.3.
Complete Feedback Behavior (FB): the robot executes all of the above controllers together simultaneously to create the full climbing behavior.

A commercially available wall (Stoneflex Stone Aggregate Panels, CEP Panels, Inc, Naperville, Illinois) consisting of small quartz gravel embedded in a resin backing was used as a climbing substrate. Although the robot normally uses lithium-polymer batteries, a supply voltage of 14.8 V was delivered via a tether for normalization purposes; however, RiSE did carry three battery packs, making the overall

weight of the robot 3.8 kg. As mentioned in Section 2.2, the target mass of the robot was 2.5 kg. A large effort to minimize the weight of the robot was put forth, but the decision to keep all processing power on the robot required that a substantial amount of the mass budget be taken up by the electronics. With a better understanding of control and sensing needs, a simplification of the onboard electronics suite will be possible. Prototype construction was also driven by readily available motor and gearbox combinations. Future systems may be able to employ lightweight custom motor and gearbox designs in order to reduce weight.

Three successive 1-m climbs were performed for each controller setup. Controllers containing traction force control had the ability to execute turning commands to keep the robot climbing straight (as in Section 4.3.2). In all other tests the robot was allowed to veer slightly until the 1-m mark was reached. If the robot slipped before reaching 1 m, the accumulated climbing distance was recorded and averaged for statistical purposes.

5.2. Experimental Results

Joint angles, motor currents, gait parameters, and forces (measured via the three-axis force sensors on each foot) were logged for each climbing run. Data were grouped by controller type, and numerical analysis was performed. Computed values are as follows:

Stance Count (SC): the desired number of legs in stance was averaged (with an associated variance). Higher values indicate a more stable gait.

Load Count (LC): the actual number of legs carrying load (defined as traction force of at least 2 N and adhesion force greater than zero). A load count close to the stance count indicates gait success, and higher values are better.

Stance Force (SF): the traction force in newtons, measured during stance averaged over time for all legs. Smaller variance is desired. Higher forces correlate with a faster robot velocity.

Velocity (V): the average robot body velocity in centimeters per second.

Distance to Failure (DF): the total distance in centimeters climbed by the robot until a failure occurred (defined as the robot falling off the wall). For climbs of less than 1 m, multiple climbs were averaged. Multiple successful climbs of 1 m accumulate distance, until a failure occurs.

The results, collected from data logs of 25 separate climbing runs totaling 37 min and 19.03 m of climbing, are shown in Table I. Three runs were performed for all of the controllers except the complete feedback behavior, FB. For each of these controllers, the robot failed at least once. Ten runs were done for the complete feedback behavior, in which the robot was run until failure, after a total of 9.6 m of climbing.

Table 1 is useful to determine the effect of each controller on climbing performance. For example, the wide variance of traction force and large discrepancy between stance count and load count indicate that OL is not very successful at climbing. T minimizes the variance of force during stance; however, it does so by modifying gait timing, and thus robot does not climb very far before slipping (note the wide variance of stance count). Not surprisingly, P achieves a better load count than O or N, but quickly slips due to bad gait timing. Note that T+GR excels in most of the calculated numerical values, particularly high stance count and load count. The complete controller

Table I. Analysis of behavioral controllers for climbing.[a]

Controller	SC ($n \leq 6$)	σ^2 (n^2)	LC ($n \leq 6$)	σ^2 (n^2)	SF (N)	σ^2 (N^2)	V (cm/s)	DF (cm)
OL	5.00	***0.00***	4.36	*0.57*	8.20	*26.00*	0.804	78.7
T	4.92	*0.60*	**5.07**	*0.56*	8.30	***10.52***	0.889	48.7
N	5.00	***0.00***	4.36	*0.45*	8.50	*25.56*	0.707	81.1
P	4.84	*0.28*	4.55	*0.51*	**8.74**	*23.51*	0.763	35.1
T+GR	**5.07**	*0.13*	5.03	***0.38***	8.20	*12.10*	0.871	293
FB	4.98	*0.20*	4.67	*0.41*	8.61	*13.16*	**0.895**	**960**

[a]Boldface indicates the best value obtained in that category. Italic type indicates the associated variance.

FB may not score as well as T+GR, but the added robustness from incorporating all control strategies together results in a behavior that climbs nearly three times as far as T+GR and an order of magnitude farther than all other control approaches.

5.3. Force Comparison

In addition to using the statistical measures above, we can see the effects of the behaviors by studying the patterns of ground reaction forces. Because several of the feedback controllers attempt to regulate the measured foot forces, there should be a difference in the "average" forces produced by feet. The force data from each stride of a foot are aggregated, and a statistical measurement of the traction force including average values, quartiles, upper and lower bounds, and statistical outliers is computed. Figures 18 and 19 show an improvement in force profiles between the open-loop gait OL and the complete feedback behavior FB.

Comparing the force profiles in Figures 18 and 19, the FB behavior seems to produce much more regular foot forces. The foot forces for OL seem jerky, taper off over a stride, and have very high upper and lower bounds. In contrast, the feedback behavior has

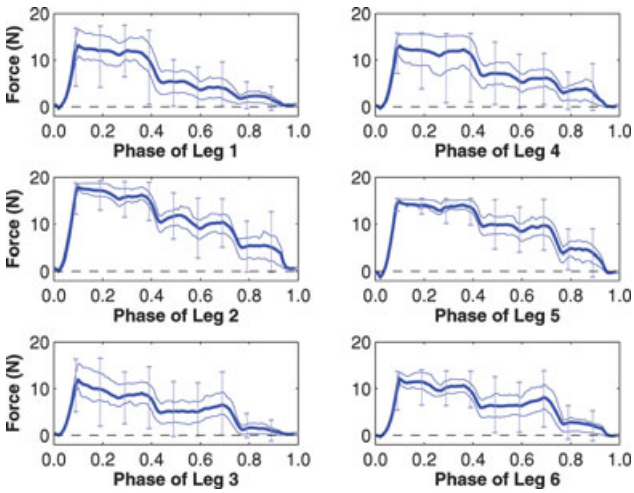

Figure 18. Traction force profiles of OL, the open-loop gait, for the six feet of the robot. Each force profile begins and ends with a recirculating foot; thus the nonzero forces in between correspond to stance. Thick center lines are average traction forces for a stride of a foot, and the thinner surrounding lines indicate quartile values. Upper and lower bounds, excluding statistical outliers, are marked every 0.1 phase.

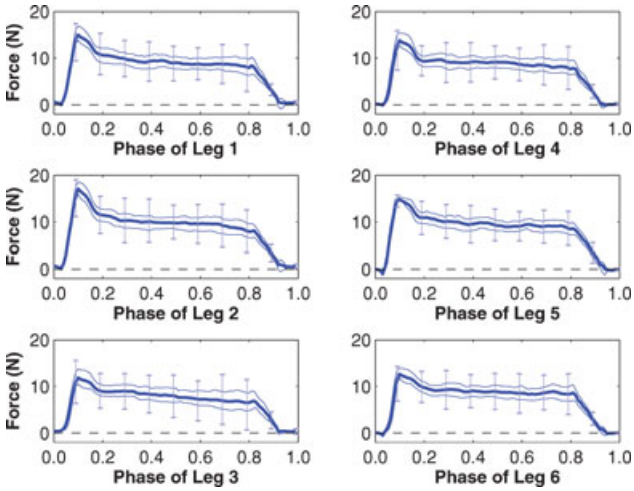

Figure 19. Traction force profiles for FB, the complete feedback behavior. As in Figure 18, the average value is surrounded by quartile values, with upper and lower bounds marked occasionally throughout. Note the smoother and tighter visual appearance of these force profiles.

Figure 20. The RiSE robotic platform (view and detail) while completing an untethered climb of a three-story (≈12 m) concrete building, making use of the feedback behaviors described in this paper.

smoother forces with much tighter bounds throughout the entire stride.

The result of these behaviors has been demonstrated in real-world environments such as the successful untethered climb of a three-story building as shown in Figure 20. Note that during this climb as well as in the results of the experiments shown here, RiSE did not meet its target speed of 0.25 m/s while climbing. To ensure near complete reliability of contact between the feet and climbing surface, the maximum forward speed was limited. On surfaces where the attachment mechanism is more reliable (i.e., carpeted walls), RiSE is able to climb at its target speed (Saunders et al., 2006).

6. CONCLUSION AND FUTURE WORK

This paper has presented the biologically inspired design of the RiSE robot. The ability of RiSE to both walk on horizontal surfaces and climb vertical surfaces is a result of the proper design of a combination of elements including body morphology, robot/terrain interface (i.e., the tuned compliance of the feet and toes), and gait. The importance of this synergy among the various elements of the robot design is made evident not only quantitatively as shown in the Results section (where, for example, the last row of Table 1 demonstrates that the combination of the individual control behaviors has nearly an order of magnitude greater climbing success relative to any single behavior), but qualitatively as evidenced by the wide array of surfaces the RiSE can climb and the distance that it can climb without failure.

Several extensions and improvements to the robot will allow for even greater utility. The speed and versatility of the platform can be improved so that future climbing robots begin to approach the performance seen in animals. In ongoing work, a new platform with several times greater power/weight ratio is under development. At the same time, adding a body pitch DOF has been shown to greatly improve the ability of the RiSE platform to accomplish abrupt vertical–horizontal and horizontal–vertical transitions in preliminary experiments.

The robot can also become more sensate and more intelligent. The body should be equipped with proximity sensors or antennae to provide information about pose with respect to irregular surfaces. The spiny feet and toes can also be improved, using harder coated materials for the spines and adding acceleration sensors at the feet so that the spines can be used as styli, able to provide a dynamic signal that characterizes the roughness of the surface as they drag over it. At a higher level, autonomous capabilities for gait adaptation, such as switching between gaits and tuning gait parameters on-line, and trajectory planning on building surfaces should reduce and ideally eliminate the need for human guidance.

ACKNOWLEDGMENTS

The RiSE platform is the result of the ingenuity, hard work, and talent of a large number of people, including robotics and biology groups at UC Berkeley, Boston Dynamics, Carnegie Mellon, Lewis and Clark, the University of Pennsylvania, and Stanford. This work is supported by a Defense Advanced Research Projects Agency within the DSO Biodynotics Program under contract DARPA/SPAWAR N66001-03-C-8045 and N66001-05-C-8025.

REFERENCES

Altendorfer, R., Moore, N., Komsuoglu, H., Buehler, M., Brown, H. B., McMordie, D., Saranli, U., Full, R., & Koditschek, D. (2001). Rhex: A biologically inspired hexapod runner. Autonomous Robots, 11, 207.

Asbeck, A., Kim, S., Cutkosky, M., Provancher, W., & Lanzetta, M. (2006). Scaling hard vertical surfaces with compliant microspine arrays. International Journal of Robotics Research, 25(12), 1165–1179.

Autumn, K., Dittmore, A., Santos, D., Spenko, M., & Cutkosky, M. (2006). Frictional adhesion: A new angle on gecko attachment. Journal of Experimental Biology, 206, 3569–3579.

Autumn, K., Hsieh, S. T., Dudek, D. M., Chen, J., Chitaphan, C., & Full, R. J. (2006). Dynamics of geckos running vertically. Journal of Experimental Biology, 209(2), 260–272.

Balaguer, C., Gimenez, A., Pastor, J., Padron, V., & Abderrahim, C. (2000). A climbing autonomous robot for inspection applications in 3d complex environments. Robotica, 18(3), 287–297.

Bretl, T. (2006). Motion planning of multi-limbed robots subject to equilibrium constraints: The free-climbing robot problem. International Journal of Robotics Research, 25(4), 317–342.

Brooks, R. A. (1989). A robot that walks; emergent behaviors from a carefully evolved network (Memo 1091). Cambridge, MA: MIT AI Lab.

Cartmill, M. (1985). Climbing. In M. Hildebrandt, D. Bramble, K. Liem, & Wake, B. (Ed.), Functional vertebrate morphology (p. 430). Cambridge, MA: Belknap Press of Harvard University.

Cham, J. G., Bailey, S. A., Clark, J. E., Full, R. J., & Cutkosky, M. R. (2002). Fast & robust: Hexapedal robots via

shape deposition manufacturing. International Journal of Robotics Research, 21(10), 869–882.
Chen, J., Peattie, A., Autumn, K., & Full, R. (2006). Differential leg function in sprawled-posture quadrapedal trotters. Journal of Experimental Biology, 209, 249–259.
Clarifying (2006). http://www.clarifyingtech.com.vortex.
Cruse, H. (1990). What mechanisms coordinate leg movement in walking arthropods? Trends in Neurosciences, 13, 15–21.
Dürr, V. (2001). Stereotypical searching movements in the stick insect: Kinematic analysis, behavioural context and simulation. Journal of Experimental Biology, 204, 1589–1604.
Dürr, V., Krause, A., Schmitz, J., & Cruse, H. (2003). Neuroethological concepts and their transfer to walking machines. International Journal of Robotics Research, 22(3–4), 151–168.
Espenschied, K. S., Quinn, R. D., Chiel, H. J., & Beer, R. D. (1993). Leg coordination mechanisms in stick insect applied to hexapod robot locomotion. Adaptive Behavior, 1(4), 455–468.
Goldman, D., Chen, T., Dudek, D., & Full, R. (2006). Dynamics of rapid vertical climbing in cockroaches reveals a template. Journal of Experimental Biology, 209, 2990–3000.
Haynes, G. C., & Rizzi, A. (2006a). Gait regulation and feedback on a robotic climbing hexapod. In Robotics: Science and Systems (pp. 97–104). University of Pennsylvania, Philadelphia.
Haynes, G. C., & Rizzi, A. A. (2006b). Gaits and gait transitions for legged robots. In Proceedings of the IEEE International Conference on Robotics and Automation (pp. 1117–1122), Orlando, FL.
Kennedy, B., Okon, A., Aghazarian, H., Badescu, M., Bao, X., Bar-Cohen, Y., Chang, Z., Dabiri, B., Garrett, M., Magnone, L., & Sherrit, S. (2005). Lemur iib: A robotic system for steep terrain access. In 8th International Conference on Climbing and Walking Robots.
Klavins, E., & Koditschek, D. (2002). Phase regulation of decentralized cyclic robotic systems. International Journal of Robotics Research, 21, 257–276.
Koditschek, D. E., Autumn, K., Buehler, M., Cutkosky, M., Fearing, R., Full, R. J., Rizzi, A. A., & Saunders, A. (2005). Robotics in scansorial environments. In Unmanned Ground Vehicle Technology VII, part of the SPIE Symposium on Defense and Security (volume 5804, pp. 291–302), Orlando, FL.
Lal Tummala, R., Mukherjee, R., Xi, N., Aslam, D., Dulimarta, H., Xiao, J., Minor, M., & Dang, G. (2002). Climbing the walls. IEEE Robotics and Automation Magazine, 9(4), 10–19.
La Rosa, G., Messina, M., Muscato, G., & Sinatra, R. (2002). A low-cost lightweight climbing robot for the inspection of vertical surfaces. Mechatronics, 12(1), 71–96.
Norberg, R. (1986). Tree creeper climbing: Mechanics, energetics and structural adaptations. Ornis Scandinavica, 17(3), 191–209.
Poulakakis, I., Smith, J. A., & Buehler, M. (2005). Modeling and experiments of untethered quadrupedal running with a bounding gait: The Scout ii robot. International Journal of Robotics Research, 24(4), 239–256.
Provancher, W., Clark, J., Geisler, W., & Cutkosky, M. R. (2005). Towards penetration-based clawed climing. In Climbing and walking robots (pp. 961–970). Berlin: Springer.
Saunders, A., Goldman, D. I., Full, R. J., & Buehler, M. (2006). The RiSE climbing robot: Body and leg design. In SPIE Unmanned Systems Technology VIII (volume 6230), Orlando, FL.
Spagna, J., Goldman, D., Lin, P., & Koditschek, D. (2007). Distributed mechanical feedback simplifies control in arthropods and robots. Bioinspiration and Biomimetics, 2, 9–18.
Spenko, M., Cutkosky, M., Majidi, C., Fearing, R., Groff, R., & Autumn, K. (2006). Foot design and integration for bioinspired climbing robots. In SPIE Unmanned Systems Technology VIII (volume 6230), Orlando, FL.
Weiss, L. E., Merz, R., Prinz, F., Neplotnik, G., Padmanabhan, P., Schultz, L., & Ramaswami, K. (1997). Shape deposition manufacturing of heterogenous structures. Journal of Manufacturing Systems, 16(4), 239–248.
Xiao, J., Morris, W., Chakravarthy, N., & Calle, A. (2006). City climber: A new generation of mobile robot with wall-climbing capability. In G. R. Gerhart, C. M. Shoemaker, & D. W. Gage (Eds.), In SPIE Unmanned Systems Technology VIII (volume 6230), Orlando, FL.
Xu, Z., & Ma, P. (2002). A wall-climbing robot for labeling scale of oil tank's volume. Robotica, 20(2), 203–207.
Zani, P. (2000). The comparative evolution of lizard claw and toe morphology and clinging performance. Journal of Evolutionary Biology, 13, 316–325.
Zhu, J., Sun, D., & Tso, S. (2002). Development of a tracked climbing robot. Journal of Intelligent and Robotic Systems, 35(4), 427–444.